

# Deflation Techniques for Stellarator Equilibrium and Optimization

Dario Panici<sup>1†</sup>, Byoungchan Jang<sup>2</sup>, Rory Conlin<sup>2</sup>, Daniel Dudt<sup>3</sup>,  
Yigit Gunsur Elmacioglu<sup>1</sup>, Egemen Kolemen<sup>1‡</sup>

<sup>1</sup>Princeton University, Princeton, New Jersey 08544, USA

<sup>2</sup>Institute for Research in Electronics and Applied Physics, University of Maryland, College Park, MD, 20742, USA

<sup>3</sup>Thea Energy, USA

Stellarator optimization is a multi-objective, non-convex problem characterized by a complex objective landscape containing many local minima. The solution resulting from a single optimization is highly sensitive to factors such as the initial guess, objective weights, and the optimization method employed. However, merely varying these factors does not guarantee that a physically distinct minimum will be found; optimizations often fail to converge to good minima or simply return to the same or very similar local minima despite large-scale parameter scans. This paper presents a novel application of deflation methods to effectively explore this landscape. By modifying the objective function to penalize and "deflate" away already-found solutions, this technique encourages the optimizer towards attractive, distinct new minima while using a single initial guess and optimization setup. We provide a primer on deflation for nonlinear systems and non-convex optimization before applying it to non-axisymmetric equilibrium and stellarator optimization problems. Key results include the discovery of families of global equilibria with similar core characteristics and the convergence to helical core equilibria without prescient initial guesses. Furthermore, we demonstrate that augmenting stage-one stellarator and stage-two coil optimization with deflation constraints readily produces multiple high-quality, distinct solutions, establishing the method's efficacy and ease of use.

## 1. Introduction

Nuclear fusion energy is a promising potential carbon-free energy source. Attaining fusion on Earth through the toroidal magnetic confinement approach involves using strong magnetic fields to confine hot plasmas in toroidally-shaped vessels. In designing a magnetically-confined nuclear fusion reactor, care must be taken to ensure that the plasma is well-contained and not lost, which hinders energy production and can cause damage to the device walls. The tokamak, a leading toroidal magnetic fusion concept, attains excellent neoclassical confinement of the plasma due to its axisymmetry, but this comes at the cost of requiring significant plasma current to provide the confining rotational transform, current which is conventionally driven inductively. Stellarators, on the other hand, attain rotational transform through 3-D shaping of the externally-generated magnetic field, dropping the requirement of large plasma currents and more readily enabling stable, steady state operation (Boozer 2005; Helander 2014). However,

† Email address for correspondence: dpanici@princeton.edu

‡ Email address for correspondence: ekolemen@princeton.edu

the loss of a physical symmetry direction means particles are no longer as well-confined as they are in tokamaks, and so stellarators require careful optimization to recover good confinement (Boozer 1983). Beyond confinement, many other considerations must be taken into account when designing a stellarator, such as stability, coil complexity, and fast particle losses. In sum, stellarator optimization is a multi-objective problem with many degrees of freedom (Landreman & Boozer 2016), and typically one deals with nonconvex objective landscapes with multiple local minima.

Even in the ideal MHD equilibrium problem alone (Freidberg 2014), at finite pressure it has been observed that multiple solutions to a given set of fixed-boundary inputs (last closed flux surface, pressure, and rotational transform profiles) can exist (Cooper *et al.* 2010), with the obtained solution depending on the initialization of the equilibrium geometry in the equilibrium solver (such a VMEC (Hirshman & Whitson 1983) or DESC (Dudt & Kolemen 2020; Panici *et al.* 2023; Conlin *et al.* 2023; Dudt *et al.* 2023)). Additionally, in recent work (Panici *et al.* 2025b), a new approach to solving for ideal MHD equilibria consistent with near-axis-expansion (NAE) solutions has been shown to be under-constrained compared to the traditional fixed-boundary problem, which would logically mean that multiple solutions may exist in this case as well.

In each of these situations, the typical approaches to find multiple distinct minima include repeatedly solving while varying the initial condition (sometimes with the use of a reduced model like the NAE (Garren & Boozer 1991; Landreman 2022; Rodriguez *et al.* 2023)), or solving from the same initial condition but while varying some hyperparameters in the objective function (such as objective targets or relative weights between objectives)(Bindel *et al.* 2023; Laia *et al.* 2026).

This paper introduces the application of deflation techniques to find multiple solutions to non-axisymmetric equilibrium and stellarator optimization problems. In Section 2, a brief introduction to deflation methods will be given, as well as their applications to nonlinear system solving and nonconvex optimization. Section 3 then will apply these techniques to find multiple equilibrium solutions to the near-axis-constrained equilibrium problem (Panici *et al.* 2025b) and to the helical core equilibrium problem (Cooper *et al.* 2010), showing its utility in finding distinct solutions when multiple valid equilibrium states may exist. Section 4 utilizes deflation in stage-one stellarator optimization and stage-two coil optimization, to demonstrate that deflation can effectively find multiple attractive local minima to these nonconvex, multi-objective optimization problems, as well as introduce and motivate a novel form of multiple-deflation. Finally, Section 5 will conclude with a discussion of the results, as well as ways to improve upon this work. While deflation methods have been applied in tokamak literature to find multiple solutions to the Grad-Shafranov equations (Ham & Farrell 2024; Pentland *et al.* 2025), to the authors' knowledge this work marks the first application of deflation to stellarators.

## 2. Deflation Methods

### 2.1. Application to Nonlinear System Solving

When dealing with nonlinear equations (or systems of nonlinear equations), multiple solutions may exist (e.g.  $\cos(x) = x^2$ ). Typically one employs a rootfinding algorithm such as Newton's method to solve such equations, which can effectively find single roots, but is limited in that it will only find a single root from a single given initial guess. Furthermore, which root is found can depend on the initial guess used for the rootfinding. In Wilkinson (1963), deflation methods were introduced to find multiple roots to polynomial equations from the same initial guess through the introduction of a barrier around known roots,

which Brown & Gearhart (1971), extended to systems of nonlinear equations. In deflation methods, once a single solution to the system of equations is found, the system is modified in such a way that the rootfinding may be re-applied to yield additional, distinct solutions to the system. More concretely, let

$$\mathbf{F}(\mathbf{x}) = 0 \quad (2.1)$$

where  $\mathbf{F}$  is the nonlinear system of equations being solved and  $\mathbf{x}$  is the state vector of unknowns. The deflation algorithm works by attempting to find a set of distinct solutions  $\{\mathbf{x}_1^*, \mathbf{x}_2^*, \dots\}$ . Suppose a solution is found  $\mathbf{x}_1^*$  to the above equation (by application of Newton's method, or some other way such as minimization of the residual). To find more solutions, one may apply a deflation operator to modify the system being solved, instead solving

$$M(\mathbf{x}; \mathbf{x}_1^*) \mathbf{F}(\mathbf{x}) = 0 \quad (2.2)$$

where

$$M(\mathbf{x}; \mathbf{x}_1^*) = \left( \frac{1}{\|\mathbf{x} - \mathbf{x}_1^*\|_2^p} \right) + \sigma \quad (2.3)$$

is the deflation operator with power and shift<sup>†</sup> parameters  $p > 0$  and  $\sigma > 0$ , respectively, and  $\|\cdot\|_2$  is the Euclidean norm. Under modest regularity conditions (Farrell *et al.* 2015; Pentland *et al.* 2025), solving the deflated system ensures the nonlinear solver does not return the known solution  $\mathbf{x}_1^*$  (from the same initial guess) but rather a distinct solution  $\mathbf{x}_2^*$  (if the nonlinear solver converges, which is not always guaranteed). To find further solutions, the system can then be deflated again using known solutions  $\{\mathbf{x}_1^*, \dots, \mathbf{x}_N^*\}$  by simply applying the deflation operator repeatedly:

$$\prod_{i=1}^N M(\mathbf{x}; \mathbf{x}_i^*) \mathbf{F}(\mathbf{x}) = 0 \quad (2.4)$$

With this deflation method, one may find multiple solutions to a given system of equations. In this work, it will be applied to find multiple solutions to various equilibrium problems in DESC, where the nonlinear system being solved is the ideal magneto-hydrodynamic (MHD) equilibrium force balance, and minimization techniques are applied to find the solutions to the unmodified and modified systems.

It is important to note that one has a choice in which part of the state (e.g. the equilibrium boundary or axis shape, a coil's geometry or current) to use in the operator  $M(\mathbf{x}; \mathbf{x}_i^*)$ . It can be useful to not always use the entire state in the deflation, especially if one has some intuition on what part of the state should be distinct. The part of state used in the deflation operator will be explicitly stated in each application in this paper. For the values of  $\sigma$  and  $p$  used, prior works have reached varying conclusions as to the effect of varying the deflation hyperparameters on the results. Farrell *et al.* (2015) found that the choice of hyperparameters can affect how many distinct solutions are successfully found through deflation, and this choice varied across different nonlinear problems. Pentland *et al.* (2025) had similar conclusions, and chose hyperparameters for each individual problem based on which performed best. Riley *et al.* (2025), on the other

<sup>†</sup> Farrell *et al.* (2015) added the shift parameter, which helps stabilize the deflation algorithm, which was otherwise prone to divergence and instability as found by Brown & Gearhart (1971) and Wilkinson (1963).

hand, reported no meaningful performance sensitivity with respect to hyperparameters or deflation operators in the problems investigated there. In this work the results were found to be relatively sensitive to the hyperparameters, especially to the shift parameter (in the context of deflated equilibrium solves, Section 3 and Subsection 3.2), with larger shift parameters resulting in finding solutions which had better equilibrium force balance errors and were less prone to being pathological minima (such as having very sharp or self-intersecting surfaces). As such, the values of  $p$  and  $\sigma$  used in each section are the ones found to provide the best performance for that specific problem, and will be stated explicitly.

## 2.2. Application to Optimization Problems with Multiple Minima

The deflation method can also be applied to optimization (Tarek & Huang 2022; Papadopoulos *et al.* 2021; Riley *et al.* 2025), where unless one is dealing with very specialized cases like convex functions, multiple local minima generally exist. Global optimization of nonconvex functions is an extremely difficult problem, and so local optimizers are still the tool of choice when facing nonconvex optimization problems (Nocedal & Wright 1999). Due to their nature, local optimization methods can only find local minima, and the found minima depend on the initial point (as well as the hyperparameters of the given optimization method). This is an analogous situation to the one in which the deflation method has already been applied above. However, in the optimization case it can also be useful to formulate the deflation operator as a nonlinear constraint, instead of using it to directly modify the objective function being minimized. To be clearer, we deal with the general optimization problem

$$\begin{aligned} \min_{\mathbf{x}} \quad & g(\mathbf{x}) \\ \text{s.t. } & c_i(\mathbf{x}) = 0 \quad , \quad d_j(\mathbf{x}) \leq 0 \end{aligned}$$

where  $g(\mathbf{x})$  is the objective function,  $c_i(\mathbf{x}) = 0$  are equality constraints and  $d_j(\mathbf{x})$  are inequality constraints. In the formulation of Tarek & Huang (2022), the deflation operator is added as an additional (nonlinear) inequality constraint defined as  $M(\mathbf{x}; \mathbf{x}_1) \leq r$  where  $r$  is some chosen maximum value for  $M(\mathbf{x}; \mathbf{x}_1)$ , and is equivalent to constraining the solution to lie outside of some region around the known solution  $\mathbf{x}_1^*$ , since the deflation constraint can be written as:

$$\|\mathbf{x} - \mathbf{x}_1^*\|_2^p \geq \frac{1}{r - \sigma} \quad (2.5)$$

This form of deflation will be used in this work to find multiple minima to various stellarator optimization problems in DESC, specifically stage-one and stage-two optimization, as it is easily added to existing optimization codes by simply augmenting the objective (to add a penalty term enforcing this constraint) or adding to the nonlinear constraints. Other deflation methods tailored for nonlinear least squares problems entail modifying the optimization algorithm itself, as is done in Riley *et al.* (2025) and was shown to increase robustness, the application of which to stellarator optimization will be the subject of future work.

### 3. Finding Multiple Solutions to non-axisymmetric Ideal MHD Equilibrium Problems

#### 3.1. Finding Multiple Solutions to the NAE-constrained Equilibrium Problem

One can consider the NAE-constrained equilibrium problem as the following system to be solved:

$$\mathbf{f}(\mathbf{x}) = 0 \quad \text{s.t. } A_{NAE}\mathbf{x} = \mathbf{b}_{NAE} \quad (3.1)$$

where  $A_{NAE}$  and  $\mathbf{b}_{NAE}$  encapsulate the linear NAE-constraints on the Fourier-Zernike coefficients  $\mathbf{x}$  which describe the equilibrium solution, and  $\mathbf{f}$  is the ideal MHD equilibrium force balance error evaluated at collocation nodes (Panici *et al.* 2023). Like any inverse equilibrium solver, DESC must begin from some initial coordinate mapping  $\mathbf{x}_0$ , from which the minimization procedure will proceed to produce an ideal MHD equilibrium solution  $\mathbf{x}^*$  s.t.  $\mathbf{f}(\mathbf{x}^*) = 0$ . In reality, due to the general non-existence of non-axisymmetric fields with nested flux surfaces, as well as the finite numerical resolutions employed,  $\mathbf{f}(\mathbf{x}^*) \neq 0$ , but rather  $\approx 0$ , but this caveat is not an issue here. One simply seeks equilibria in the usual way in DESC, as local minima of the system of residuals being minimized.

The initial coordinate mapping  $\mathbf{x}_0$  will be taken as the Fourier-Zernike fit of the flux surface geometry evaluated from the NAE (obtained using pyQSC or pyQIC). The NAE-constrained equilibrium problem 3.1 is then solved as usual in order to obtain the first solution  $\mathbf{x}_1^*$ . To find further solutions, one then solves the deflated equilibrium problem:

$$\prod_i M(\mathbf{x}; \mathbf{x}_i^*) \mathbf{f}(\mathbf{x}) = 0 \quad \text{s.t. } A_{NAE}\mathbf{x} = \mathbf{b}_{NAE} \quad (3.2)$$

where the deflation operator  $M$  ensures that, if a solution is found, it will be distinct from the past solutions. Because of the caveat that solutions  $\mathbf{f} = 0$  are not typically found but rather  $\mathbf{f} \approx 0$ , once a solution  $\mathbf{x}_i$  to Equation 3.2 is found, that solution is used as an initial guess and the non-deflated problem Equation 3.1 is solved to yield the solution  $\mathbf{x}_i^*$ . This is done to ensure that  $\mathbf{x}_i^*$  is actually a solution to the NAE-constrained equilibrium problem, and not merely some local minimum of the deflated equilibrium problem. So effectively, the deflated solve is done only to find an initial condition near a new local minimum of Equation 3.1. This is summarized in Algorithm 1. In this section, the deflation operator was applied to the boundary Fourier coefficients of the solution, e.g. on  $R_{mn}^b, Z_{mn}^b$ , and the power and shift parameters used were  $p = 2$  and  $\sigma = 500$ . These power and shift were chosen as they were found to work best after performing a small parameter scan. Having a larger shift was found to especially be important for finding equilibria which did not suffer from poor force balance due to the deflation cost being dominant over the equilibrium force cost.

To provide an example, we take the first-order quasi-axisymmetric (QA) NAE solution from Panici *et al.* (2025b). We evaluate the NAE surfaces at  $r = 0.25m$  (for an aspect ratio of  $\sim 4$ ), at equilibrium radial, poloidal, and toroidal resolution of  $L = 12, M = 4, N = 8$ , respectively. We follow the above procedure, first finding an NAE-constrained solution, then performing deflated NAE-constrained solves to find initial conditions from which to then find new NAE-constrained solutions. We apply this procedure 25 times to result in 25 distinct NAE-constrained solutions. Like in Panici *et al.* (2025b), after each NAE-constrained equilibrium solve, we then solve a conventional fixed-boundary equilibrium solve to ensure equilibrium in the traditional sense, and we note that every presented solution here has a volume averaged force balance error below one percent. The NAE-

**Algorithm 1** NAE-Constrained Equilibrium Deflation

---

**Require:**  $\mathbf{x}_0$  initial coordinate mapping,  $N_{defl}$  number of deflation iterations,  $p$  power parameter,  $\sigma$  shift parameter

→Solve NAE-Constrained Equilibrium

$$\mathbf{x}_1^{NAE} = \operatorname{argmin}_x \mathbf{f}(\mathbf{x}) = 0 \text{ s.t. } A_{NAE}\mathbf{x} = \mathbf{b}_{NAE} \text{ from initial state } \mathbf{x}_0$$

→Solve Fixed-Boundary Equilibrium

$$\mathbf{x}_1^* = \operatorname{argmin}_x \mathbf{f}(\mathbf{x}) = 0 \text{ s.t. } A\mathbf{x} = \mathbf{b} \text{ from initial state } \mathbf{x}_1$$

$i = 1$

→Initialize list of solved equilibria to deflate with

eqs=[ $\mathbf{x}_1^*$ ]

**while**  $i < N_{defl}$  **do**

    →Solve Deflated NAE-Constrained Equilibrium

$$\mathbf{x}_i = \operatorname{argmin}_x \prod_i M(\mathbf{x}; \text{eqs}) \mathbf{f}(\mathbf{x}) = 0 \text{ s.t. } A_{NAE}\mathbf{x} = \mathbf{b}_{NAE} \text{ from initial state } \mathbf{x}_0$$

    →Solve NAE-Constrained Equilibrium

$$\mathbf{x}_i^{NAE} = \operatorname{argmin}_x \mathbf{f}(\mathbf{x}) = 0 \text{ s.t. } A_{NAE}\mathbf{x} = \mathbf{b}_{NAE} \text{ from initial state } \mathbf{x}_i$$

    →Solve Fixed-Boundary Equilibrium

$$\mathbf{x}_i^* = \operatorname{argmin}_x \mathbf{f}(\mathbf{x}) = 0 \text{ s.t. } A\mathbf{x} = \mathbf{b} \text{ from initial state } \mathbf{x}_i^{NAE}$$

    eqs.append( $\mathbf{x}_i^*$ )

$i = i + 1$

**end while**

**return** eqs

---

constraints used in this section were on the first-order  $R, Z$  flux surface geometries of the equilibrium. Figure 1 show the boundary shapes and magnetic axis positions for each of the found NAE-constrained solutions at two toroidal angles, while Figures 2a and 2b shows the rotational transform profiles and Boozer QS errors ( $\hat{f}_B$  (Rodríguez *et al.* 2022; Dudit *et al.* 2023)) for each solution. It can be seen that a wide range of both geometries and rotational transform profiles were found, all of which share the same axis position and on-axis rotational transform, as well as a general adherence to the expected scaling of the QS error with  $\rho^2$ . To look more closely at the different solutions found, Figure 3 shows the flux surfaces, rotational transform profiles, and QS error for two solutions, the first (i.e. undeflated) and the 21st solutions found. While both share the same magnetic axis, on-axis rotational transform, and both are QS to first-order in  $\rho$ , the sign and strength of the shear is different, as well as the outer flux surface geometries of the two equilibria. Both could serve as good initial guesses for further stage-one optimizations if one desired a QA equilibrium, with each being individually useful if one desires a different rotational transform profile (the second solution being a good point from which to optimize for larger shear, for example). Appendix A shows some further physics metrics of these QA solutions found, emphasizing the wide range of possible solutions which match similar core properties, including that some have stable magnetic wells (such as the 21st solution).

It is worth noting that when performing deflated solves, the only guarantee is that if a solution is found, the obtained state parameter values do not exactly match that of the prior deflated solutions. However, depending on how the state is parametrized, the same physical solution may correspond to multiple different sets of state parameter values. As a concrete example, a stellarator-symmetric equilibrium with  $N_{FP}$ -symmetry rotated around toroidally through the angle  $\pi/N_{FP}$  can be represented by the same stellarator-symmetric basis and appear different to the deflation operator, but have the same exact physical properties. This is not an issue for the NAE-constrained equilibria, as the fixing

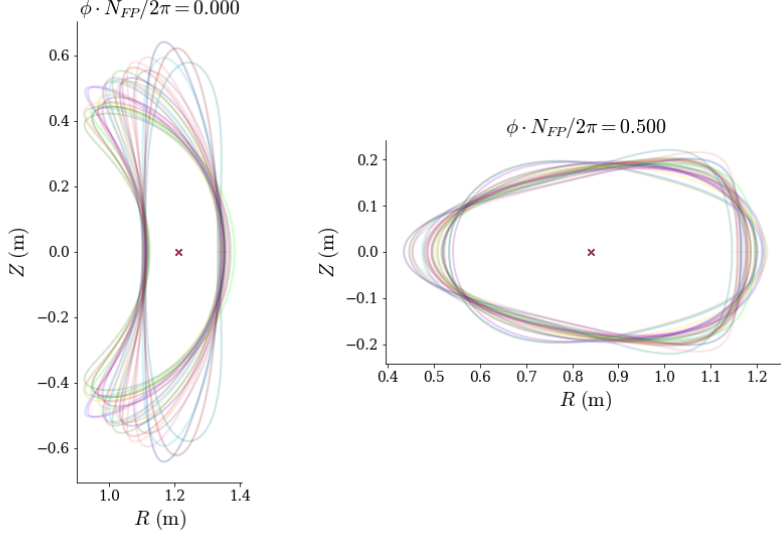


Figure 1: Boundaries at two different toroidal angles for the 25 deflated first-order NAE-constrained equilibria.

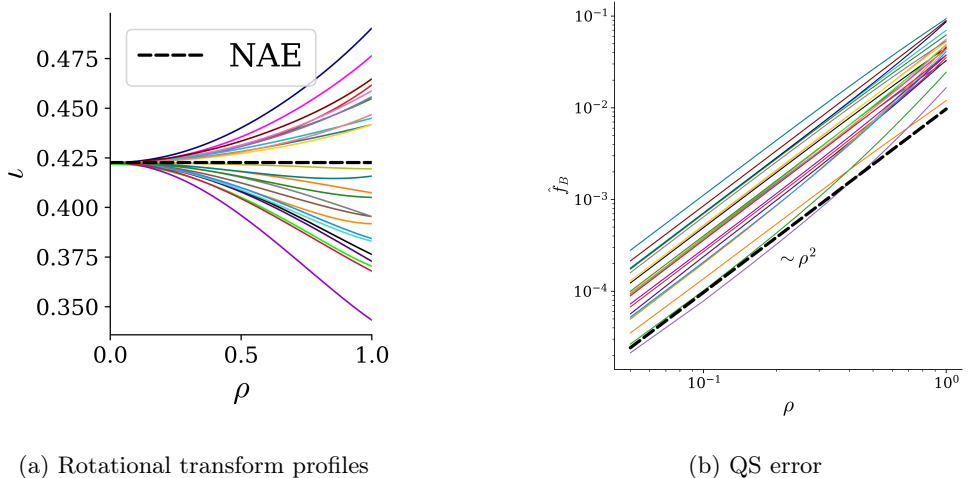


Figure 2: Rotational transform profiles and QS error for the 25 deflated first-order NAE-constrained equilibria.

of the magnetic axis removes this possible degeneracy, but it will have implications for stage one and stage two optimizations, as discussed later in Section 4.

### 3.2. Helical Core Equilibria

In Cooper *et al.* (2010), it was found that for certain profiles and axisymmetric boundaries, it was possible for ideal MHD equilibrium solvers to find two distinct equilibria, one with a wholly axisymmetric interior and one non-axisymmetric with a helically distorted magnetic axis, both having the same fixed axisymmetric boundary.

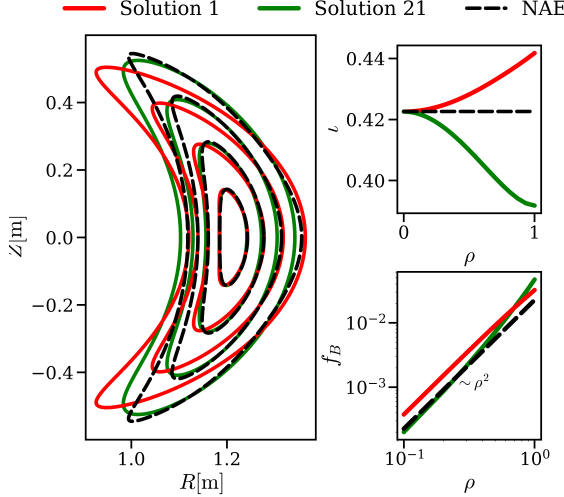


Figure 3: A comparison of two of the 25 deflated first-order NAE-constrained equilibria. (Left) The flux surfaces of the two equilibria at the  $\phi = 0$  cross-section, compared to the original NAE surfaces. (Right top) The rotational transform profile for the two solutions, with both matching well near-axis. (Right Bottom) The Boozer QS error metric for the two solutions, with both displaying the expected quadratic scaling of the QS error with  $\rho$ .

Cooper obtained the second solution by initializing the VMEC coordinate mapping with a helically perturbed magnetic axis, which then would converge to the helical core state. However, it would be interesting to find such states without the use of judiciously perturbed initial states. To approach this, we state the typical fixed-boundary equilibrium problem in DESC as

$$\mathbf{f}(\mathbf{x}) = 0 \text{ s.t. } A\mathbf{x} = \mathbf{b} \quad (3.3)$$

where here  $A$  are the linear constraints on the Fourier-Zernike coefficients  $\mathbf{x}$  which enforce the fixed-boundary geometric constraint. One may apply the deflation technique to this system:

$$\prod_i M(\mathbf{x}; \mathbf{x}_i^*) \mathbf{f}(\mathbf{x}) = 0 \text{ s.t. } A\mathbf{x} = \mathbf{b} \quad (3.4)$$

where  $\mathbf{x}_i^*$  are solutions to Equation 3.3. Like in the prior section, the procedure adopted is to first solve Equation 3.3 to obtain  $\mathbf{x}_1^*$  from some initial coordinate mapping  $\mathbf{x}_0$ , then use the same initial mapping  $\mathbf{x}_0$  to solve the deflated equilibrium Equation 3.4 to obtain  $\mathbf{x}_2$ , which is then used as an initial condition from which to solve Equation 3.3 to obtain  $\mathbf{x}_2^*$ . In this problem, because the desired additional distinct solution is one with a different magnetic axis, the deflation operator was applied only to the magnetic axis position, i.e. if the current state's magnetic axis geometry is  $\mathbf{x}_{axis}$  and the solution axis  $\mathbf{x}_{axis}^*$ , the deflation operator is  $M(\mathbf{x}_{axis}; \mathbf{x}_{axis}^*)$ . The axis position is represented as the toroidal Fourier series describing the curve, so  $\mathbf{x}_{axis} = [R_n, Z_n]$  where

$$\begin{aligned}
R_{axis}(\phi) &= R_n \mathcal{F}_n(\phi) \\
Z_{axis}(\phi) &= Z_n \mathcal{F}_n(\phi) \\
\mathcal{F}_n(\phi) &= \begin{cases} \cos(nN_{FP}\phi) & n \geq 0 \\ \sin(nN_{FP}\phi) & n < 0 \end{cases}
\end{aligned} \tag{3.5}$$

The power and shift parameters used were  $p = 2$  and  $\sigma = 100$ , again chosen as the larger shift was found to result in a more stable deflated equilibrium solve and better final equilibrium.

This procedure was applied to an equilibrium described in Cooper *et al.* (2010). The axisymmetric fixed-boundary shape, pressure and rotational transform profiles are given by

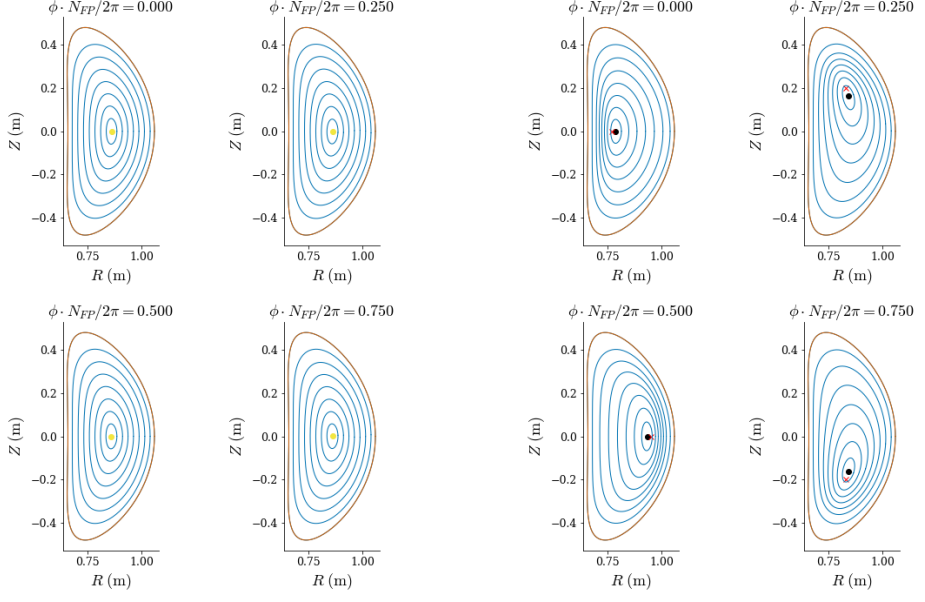
$$\begin{aligned}
R(\theta) &= 0.8 + 0.2\cos\theta + 0.06\cos 2\theta \text{ [m]} \\
Z(\theta) &= 0.48\sin\theta \text{ [m]} \\
p(\rho) &= p_0(1 - \rho^2) \\
\iota(\rho) &= 0.9 + 0.2\rho^2 - 0.8\rho^{12}
\end{aligned} \tag{3.6}$$

Where  $p_0 = 49,700$  Pa was chosen to yield a volume-averaged plasma  $\beta \approx 0.5\%$ . Figure 4 shows the flux surfaces of the axisymmetric equilibrium state  $\mathbf{x}_1^*$  on the left, and the non-axisymmetric helical core branch  $\mathbf{x}_2^*$  on the right. Each have a volume-averaged force balance error less than 1%. The right figure shows also in red the axis of the result of the deflated equilibrium solve,  $\mathbf{x}_2$ , where the deflated equilibrium solve results in an axis perturbation similar to what was found to be necessary in Cooper *et al.* (2010). It is worth reiterating this point: the helical axis state was found without any prescient choice of perturbation to the axisymmetric initial condition. Instead, the deflated equilibrium solve found the second initial condition  $\mathbf{x}_2$ , from which the equilibrium solver then converged to the helical core equilibrium  $\mathbf{x}_2^*$ . This shows the promise of deflation methods in finding effective initial conditions for cases where one may suspect multiple equilibrium states, and also warrants further search for other cases where such potential neighboring states exist.

## 4. Deflation for finding multiple local minima to nonconvex optimizations

### 4.1. Stage one

Stage-one stellarator optimization almost always have multiple local minima due to the complex, multi-objective landscapes typically explored. These multiple objectives may compete with each other (Bindel *et al.* 2023; Laia *et al.* 2026), and nonlinear constraints are usually enforced with penalty methods in combined sum of squares objectives. Constrained optimization methods have been shown to improve the situation somewhat (Conlin *et al.* 2024), but even these methods can still lead to poor local minima. Conventionally, the only recourse left is to launch many optimizations beginning from many initial conditions, or resort to global optimization methods, both of which are expensive approaches. Instead, one may apply deflation to attempt to find distinct local minima in the optimization landscape, starting from the same initial guess (Tarek & Huang 2022). In this section we employ deflation to find multiple local minima to a quasi-helically symmetric (QH) stellarator optimization problem. Constrained optimization



(a) Axisymmetric equilibrium solution.

(b) Helical core equilibrium solution.

Figure 4: The two branches of equilibrium found for the helical core state presented in Cooper *et al.* (2010). (Left) The axisymmetric equilibrium state, found when solving from an axisymmetric initial condition. (Right) The helical core equilibrium, found when solving from the deflated equilibrium solve as an the initial state. The solved equilibrium's axis is shown as a black dot, while the deflated solve solution's is a red cross, showing that the deflated equilibrium problem encouraged an axis perturbation in the correct direction, without requiring any prior insight.

using the augmented Lagrangian approach will be employed, and the deflation will be in the form of an additional nonlinear constraint.

To state the specific problem clearly, we will seek a quasi-helically symmetric vacuum stellarator. The optimization will target the two-term quasisymmetry (QS) metric (Hélander & Simakov 2008; Landreman & Paul 2022; Rodríguez *et al.* 2022), while constraining the aspect ratio, rotational transform, and ideal MHD force balance through. The two-term QS metric is given by  $f_{QS} = [(M\iota - N)(\mathbf{B} \times \nabla\psi)] \cdot \nabla B - (MG + \iota I)\mathbf{B} \cdot \nabla B^2$ , with  $\mathbf{B}$  being the magnetic field and  $B$  its magnitude,  $(M, N) = (1, 4)$  being the QS helicity,  $\psi$  being the normalized toroidal flux,  $\iota$  the rotational transform and  $I, G$  being the Boozer toroidal and poloidal currents, respectively. We fix the major radius of the equilibrium  $R_0$ , aspect ratio  $R_0/a$ , net enclosed toroidal flux  $\Psi$  and vacuum net toroidal current  $I_{tor}(\rho)$  and pressure profile  $p(\rho)$  during the solve. We then minimize this objective while constraining the average rotational transform  $\bar{\iota}$  to be between 0.7 and 0.3, as well as enforcing ideal MHD force balance. The constraints for the undeflated optimization problem are then:

$$\begin{aligned}
R_0 &= 1 \text{ m} \\
R_0/a &= 8 \\
0.7 < \bar{\iota} < 3 \\
p(\rho) &= 0 \\
I_{tor}(\rho) &= 0 \\
\Psi &= 0.04 \text{ Tm}^2 \\
\mathbf{J} \times \mathbf{B} - \nabla p &= 0
\end{aligned} \tag{4.1}$$

This problem is initially solved using the augmented Lagrangian approach outlined in Conlin *et al.* (2024) to find a solution  $\mathbf{x}_1^*$ . In this section we also employ the exponential spectral scaling (ESS) introduced by Jang *et al.* (2025) to scale the variables in the problem to respect the expected spectral decay. This spectral scaling is employed to scale not the boundary modes as was done in the original work, but instead to scale based on the Fourier-Zernike modes of the equilibrium, as in the constrained optimization approach the degrees of freedom are not just the boundary, but the entire geometry of the equilibrium<sup>†</sup>. The ESS scaling in this work used an exponent of  $\alpha = 1.2$  and the  $L^\infty$  norm.

Once  $\mathbf{x}_1^*$  is obtained, the deflated problem is solved, which is the same as the above setup but with an additional deflation constraint:

$$f_{deflation} := \prod_i M(\mathbf{x}; \mathbf{x}_i^*) \leq r \tag{4.2}$$

where  $\mathbf{x}_i^*$  are the prior solutions, and  $r$  is some positive constant (chosen to be 1 here, a scan over larger values revealed no significant difference in results), effectively pushing the optimizer away from some region around each of the already-found solutions. The deflation operator here is applied to the entire equilibrium state (the Fourier-Zernike coefficients for  $R_{lmn}$ ,  $Z_{lmn}$  and  $\lambda_{lmn}$ ), with the power and shift parameters  $p = 2$  and  $\sigma = 0$ . We begin from a simple axisymmetric circular torus initial guess with 1m major radius and 0.125m minor radius, and proceed with the deflated optimization for 30 iterations. Not every iteration is guaranteed to result in an equilibrium which satisfies all of our constraints after optimization, so we will filter the results to only those which have  $\bar{\iota}$  between 0.7 and 3, as well as filter for only equilibria with volume averaged force balances below 1%. 18 equilibria pass these filters, and their boundaries, rotational transform profiles, QS errors, and Boozer surface plots are shown in Figure 5, Figure 6a, Figure 6b, and Figure 7, respectively. The results show that the algorithm successfully found a range of equilibria with good QH and varying rotational transform profiles and boundary shapes.

However, it can be seen that some similar boundaries and equilibria were found. This is likely due to three reasons: first, the Fourier representation of a single physical boundary shape is not unique (owing to the arbitrariness of the poloidal angle), and thus there may be two state vectors which are "far" from each other in the sense of they have different Fourier coefficients, but the actual physical boundaries they describe are very similar. Use of either an explicit spectral condensation constraint (Hirshman & Breslau 1998), or

<sup>†</sup> This is in contrast to the typical stage one optimization approach where the ideal MHD force balance constraint is enforced through an equilibrium solve at each step, effectively making the interior of the equilibrium a function of the boundary only and thus the boundary DOFs are the optimization variables in that case.

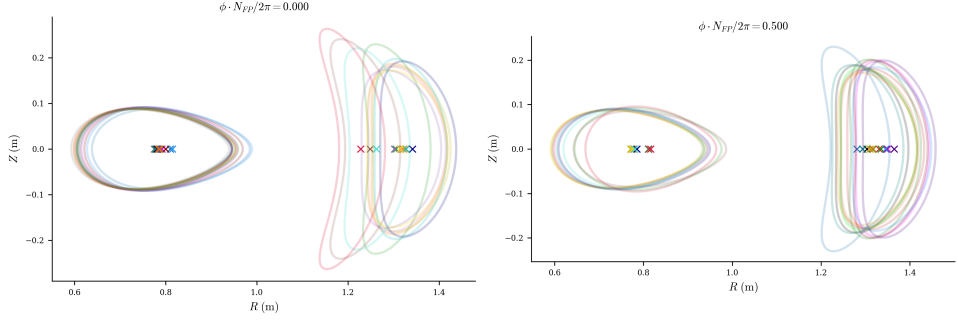


Figure 5: Boundaries at two different toroidal angles for the 18 optimized QH equilibria found through deflation which passed the filters.

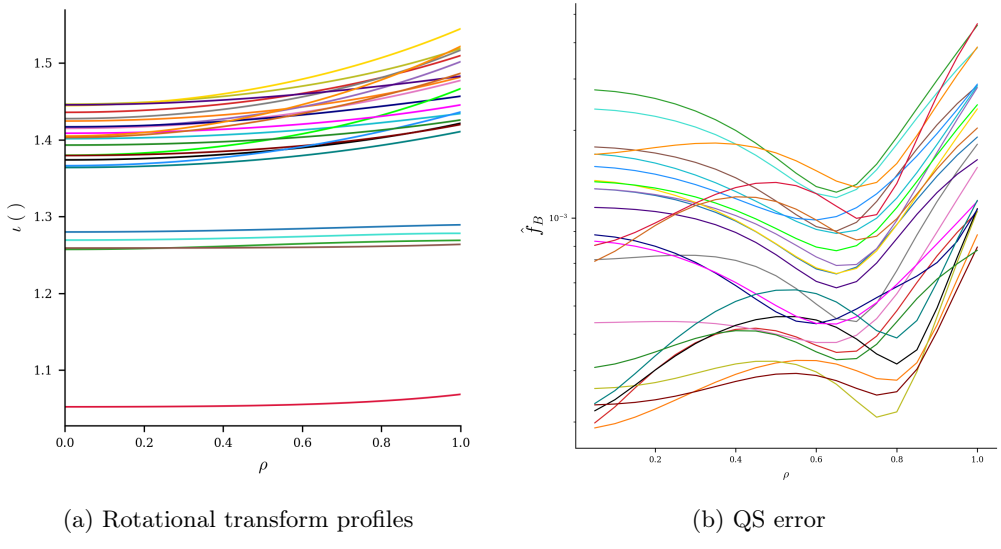


Figure 6: Rotational transform profiles and QS error for the 18 optimized QH equilibria found through deflation which passed the filters.

enforcing a poloidal angle representation that is less degenerate (Henneberg *et al.* 2021) may alleviate this issue<sup>‡</sup>.

<sup>‡</sup> It should be noted that in DESC, spectral condensation is implicitly attained through the freedom afforded to the poloidal stream function, as shown in Panici *et al.* (2023), where the spectral width of the DESC solution is found to be comparable to VMEC. This however does

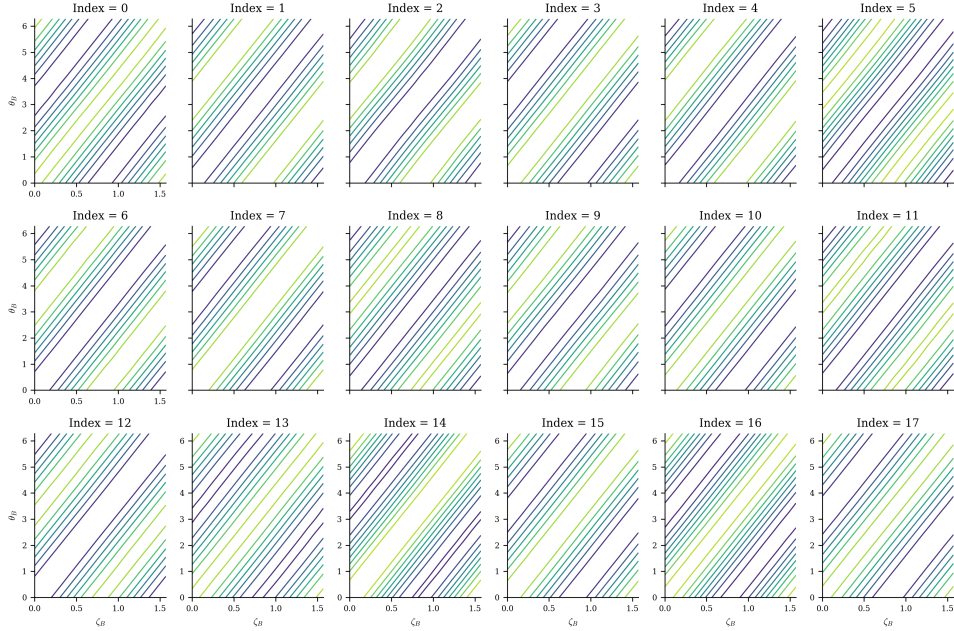


Figure 7: Magnetic field magnitude contours in Boozer coordinates on the boundary for the 18 optimized QH equilibria found through deflation which passed the filters.

The second reason is that the same exact physical boundary may, in stellarator-symmetry, be described by the same poloidal angle definition in two different ways, as one may simply shift the toroidal angle in the boundary definition by  $\pi/N_{FP}$  to obtain the same physical boundary, but now offset toroidally, similar to the two equilibria in the filtered set shown in Figure 8. This problem is not present in Subsection 3.1, as fixing the axis and near-axis behavior prevents such shifts. However in Subsection 3.2 this problem can and was observed to occur (that is, if one were to run a deflated equilibrium solve using as deflated states the axisymmetric and the helical core state, one would find the helical core state rotated by  $\pi$  radians toroidally). A method which could be used to avoid this is to also add the toroidally shifted counterparts of found solutions to the set of deflated states to prevent the other potential parametrization of the same physical solution from being found by the optimizer. Note that if the assumption of stellarator symmetry is relaxed, this problem may be much worse, as now any arbitrary toroidal rotation of the boundary can be found, yielding the same physical solution but still being "far" from the deflated solutions in coefficient space. In practice, the relaxation of stellarator symmetry will likely necessitate more deflation iterations to find meaningfully distinct solutions than in the stellarator symmetric case. While the work presented in this paper assumes stellarator symmetry, the implemented deflation methods can work as well as asymmetric cases (with the aforementioned caveats on their effect on the problem). Stellarator symmetry was simply assumed in this work for convenience.

The third reason may be due to the form of multiple-deflation used in the problem, along with the choice of  $\sigma = 0$  for the shift parameter. When deflating multiple solutions, the deflation operators for each individual solution are multiplied together. While this not solve the degeneracy issue completely, as multiple different poloidal angles may be similarly spectrally condensed.

is the method that makes the most sense for nonlinear rootfinding (where one then multiplies the deflation operator by  $\mathbf{f}$  and seeks  $M\mathbf{f} = 0$ ), in the present case of using the deflation operator as a nonlinear constraint, it may lead to unexpected and unwanted behavior as the number of deflated solution increases. This is because as more solutions are added, the extra cost in the problem due to deflation can be artificially damped by virtue of the existence of more diverse solutions. To put this more concretely, if we have 2 existing solutions  $\mathbf{x}_1^*$  and  $\mathbf{x}_2^*$ , our deflation operator with those two deflated states is given (with  $\sigma = 0$  and  $p = 2$ ) as  $m(\mathbf{x}; \{\mathbf{x}_1^*, \mathbf{x}_2^*\}) = \frac{1}{|\mathbf{x} - \mathbf{x}_1^*|^2} \frac{1}{|\mathbf{x} - \mathbf{x}_2^*|^2}$ , and our deflation constraint is (as was chosen in this problem)  $m \leq r$  and  $r = 1$ . If a given  $\mathbf{x}$  is such that  $\frac{1}{|\mathbf{x} - \mathbf{x}_1^*|^2} = 2$ , then that state would be avoided in the first deflation iteration because  $m(\mathbf{x}; \mathbf{x}_1^*) > r$ . However, in the second deflation iteration, if that same state  $\mathbf{x}$  now happens to be far from  $\mathbf{x}_2^*$  such that  $\frac{1}{|\mathbf{x} - \mathbf{x}_2^*|^2} = 0.25$ , then the deflation cost becomes  $m(\mathbf{x}; \{\mathbf{x}_1^*, \mathbf{x}_2^*\}) = 0.5$  which is below the set bound of  $r = 1$ , thus this state is no longer avoided. This is an unintuitive result, and can change the shape of the optimization landscape as the deflation progresses in potentially undesired ways. Not only does the expected and desired change of adding more barriers around other found solutions occur, but now we also are modifying the existing barriers, potentially allowing previously disallowed solutions simply due to the formulation of the constraint. This is schematically shown in Figure 9, where the white contour is the contour within which the deflation constraint is violated, and it can be seen from the first panel to the second that the addition of the second deflated solution reduces the size of the excluded region around the original deflated solution. One may avoid this unintuitive modification of the landscape by choosing to handle multiple-deflation with a sum instead of a product, i.e.

$$m_{sum}(\mathbf{x}; \{\mathbf{x}_i^*\}) = \sum_i \left( \frac{1}{|\mathbf{x} - \mathbf{x}_i^*|^2} + \sigma \right) \quad (4.3)$$

or, to avoid the accretion of the cost due simply to the accumulation of  $\sigma$ , using only a single shift (as first proposed by Riley *et al.* (2025)):

$$m_{sum}(\mathbf{x}; \{\mathbf{x}_i^*\}) = \sigma + \sum_i \frac{1}{|\mathbf{x} - \mathbf{x}_i^*|^p} \quad (4.4)$$

This form of the multiple deflation operator, which we will call the "sum-reduction" deflation operator, will be used in the next section on stage-two optimization to avoid the problems outlined in this section. The rightmost panel of Figure 9 shows that with the sum-reduction deflation operator, the excluded region no longer shrinks in size when the second deflated solution is included. One could also choose to increase the bound proportional to the amount of solutions being deflated, offering a more controlled way to modify the infeasible region sizes compared to the product-reduction operator.

#### 4.2. Stage-two Filamentary Coil Optimization

Like stage-one optimizations, stage-two filamentary coil optimizations are notoriously nonconvex problems that can have many local minima. Once again, we will apply the deflation operator as a constraint during optimization to find multiple local minima, this time using the "sum-reduction" deflation operator of Equation 4.3 to deal with multiple deflations. We will find coils for the vacuum precise QA stellarator, using a stellarator-symmetric coilset with four coils per half-field period. We parametrize the coil geometry as filamentary curves with Fourier series for the X, Y and Z components of the curves, as first done by FOCUS (Zhu *et al.* 2018b,a), using Fourier modes up to fifth order in the

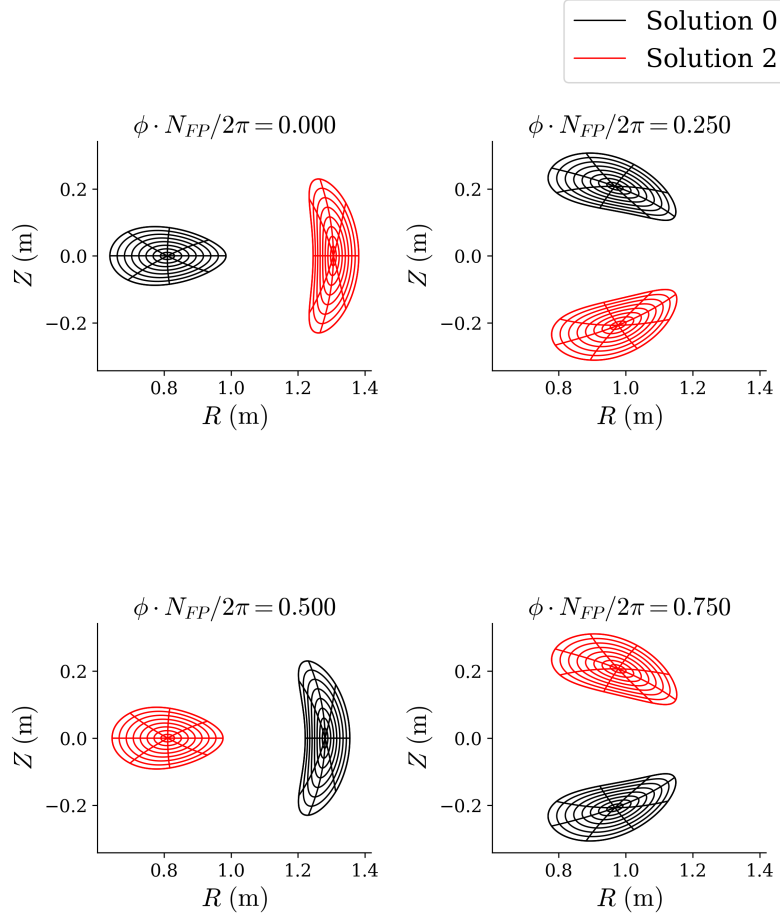


Figure 8: Two of the found QH solutions from subsection 4.1, the first (index 0, i.e. undeflated) solution and the third (index 2) solution. It can be seen that the equilibria are nearly physically identical aside from a  $\pi/N_{FP}$  toroidal rotation, which motivates the inclusion of rotated solutions in the deflation to avoid such degenerate solutions.

curve parameter  $t$ . The least-squares augmented Lagrangian approach in DESC is again used to perform the coil optimization, similar to the approach taken in Gil *et al.* (2025). The ESS scaling is also applied here to the Fourier components of the coil geometry. The objective being minimized is the quadratic flux on the last closed flux surface:

$$f_{B_n} = \int_S (\mathbf{B} \cdot \mathbf{n})^2 dA \quad (4.5)$$

where  $\mathbf{B}$  is the coil-generated magnetic field,  $\mathbf{n}$  is the unit surface normal,  $S$  is the last closed flux surface and  $dA$  is the local surface element. This objective is then minimized subject to a set of constraints on the coil geometries and currents, specifically:

- The coil currents are constrained such that their sum matches the necessary poloidal

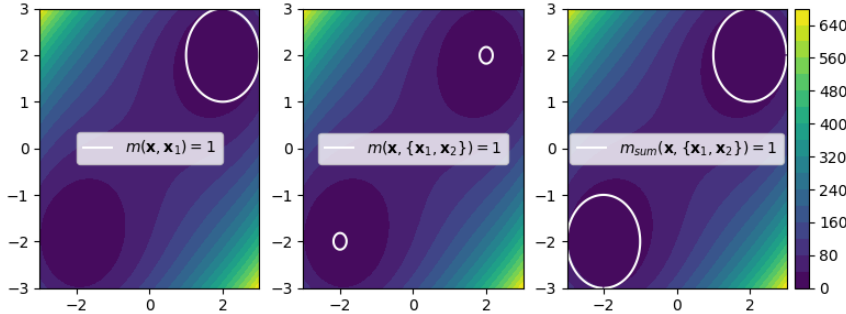


Figure 9: Each panel shows the shaded contours of the function  $f(x, y) = ((x - 2)^2 + (y - 2)^2)((x + 2)^2 + (y + 2)^2)$ , and in each panel in white is the level set corresponding to 1 of (left) the deflation operator acting only on a single deflated minimum  $(x, y) = (2, 2)$ , and the deflation operator acting on two minima,  $(2, 2)$  and  $(-2, -2)$  (middle) with the conventional product-reduction deflation operator, and (right) with the sum-reduction operator. The regions inside the white contours would be infeasible states for the deflated optimization problem, and it can be seen that while the infeasible region around  $(2, 2)$  is modified when the additional state is added with the product-reduction deflation operator in the middle plot, the sum-reduction operator in the right plot retains the infeasible region of the original deflated state, a more intuitive modification of the optimization landscape.

linking current demanded by the equilibrium, ensuring the field magnitude matches and also avoiding the trivial solution of zero current (Panici *et al.* 2025a).

- The coil-coil minimum distance is bounded to  $d_{cc} \geq 0.09$  m.
- The coil-plasma minimum distance is bounded to  $d_{cp} \geq 0.2$  m.
- The pointwise coil curvature  $\kappa$  is bounded to be between  $-8 \text{ m}^{-1}$  and  $8 \text{ m}^{-1}$  to discourage excessive coil shaping.
- Each individual coil length is bounded to be less than 6.5 m. This differs from the conventional sum of lengths constrained to a target length used in stage-two optimization (Zhu *et al.* 2018b; Wechsung *et al.* 2022; Kaptanoglu *et al.* 2025; Gil *et al.* 2025). Constraining individual coil lengths was found to work better, as when only the length sum is constrained, feasible solutions include coilsets where a single coil gets very long, which is usually not a desired solution engineering-wise.
- The variance of the incremental coil arclength,  $\text{var}(\boldsymbol{\Gamma}'(t))$  is constrained to be zero, similar to the constraint proposed by Wechsung *et al.* (2022), where it is argued that such a constraint may reduce the inherent degeneracy in the curve parametrization. This is particularly important for this work because, as previously discussed, degeneracy in parametrization may hinder deflation. Practically, this variance will not be zero, but will at least be penalized to remain small.

A grid of 101 points evenly spaced in the curve parameter  $t$  is used to discretize the coil for purposes of the Biot-Savart law and any other coil geometry computations, and a stellarator-symmetric grid of 51 poloidal and 101 toroidal points on the plasma surface is used for evaluating the quadratic flux and coil-plasma distance objectives. An additional deflation constraint is then added using the sum-reduction form given in Equation 4.3, with  $\sigma = 0$  and  $p = 2$ , and the part of state used for deflation will be the Fourier

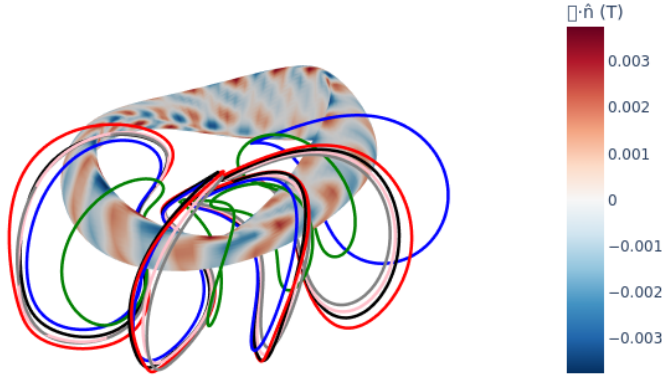


Figure 10: The unique coils in each of the 6 optimized filamentary coilsets for the vacuum precise QA configuration. The normal field error from the first optimized coilset is shown on the equilibrium surface.

coefficients of the coil geometries. The value of this deflation metric is constrained to be less than 1:

$$m_{sum}(\mathbf{x}; \{\mathbf{x}_i^*\}) \leq 1 \quad (4.6)$$

We first run the optimization without the deflation constraint, then perform five additional optimizations including the deflation constraint. We find six different coilsets, which we show visually in Figure 10 and compare the properties of each in Table 1.

It can be seen that all but one of the coilsets satisfy the constraints and achieve good normal field errors (Kappel *et al.* 2024). The index-4 coilset with distinctly worse normal field error is the only one which failed to satisfy the constraints, including the deflation constraint, indicating that given the initial guess and optimizer settings used, it could not find a feasible solution. It is especially interesting that physically, this coilset (in green in Figure 10) seems to be the most visually distinct from the others, showing that the parametrization degeneracy issue is perhaps not entirely solved with the use of the arclength variance penalty included in this problem.

## 5. Conclusions and Future Work

In this work, the deflation method was introduced and successfully applied to stellarator equilibrium and optimization problems to find multiple solutions and local minima. The deflation method offers an additional tool for exploring the complex objective landscapes which characterize both stellarator optimization and non-axisymmetric equilibrium solves, beyond the conventional approaches of launching the same optimization with many different initial guesses (which can be wasteful, as many may converge to the same or similar local minima) or tinkering with objective weights (which can be

Coilset	$\frac{\langle B_n \rangle}{ B }$	$d_{cc}$ [m]	$d_{cp}$ [m]	$\kappa_{max}$ [ $m^{-1}$ ]	Max Coil Length [m]	$Var(\mathbf{f}'(t))$ [ $m^2$ ]
0	1.011e-03	0.1465	0.2684	3.5612	4.8419	2.948e-03
1	6.719e-04	0.1304	0.2930	3.5944	5.2340	1.911e-03
2	1.393e-03	0.1545	0.2752	3.3720	4.8624	4.319e-03
3	1.263e-03	0.1495	0.2731	3.4583	4.8911	4.013e-03
4	2.327e-02	0.1443	0.2001	5.0100	3.6251	1.702e-02
5	1.806e-03	0.1541	0.2525	3.3786	4.5227	5.518e-03

Table 1: Figures of merit for the 6 optimized coilsets found through the deflation algorithm, where  $\frac{\langle B_n \rangle}{|B|}$  denotes the average normalized normal field error over the plasma surface, with the normalizing field as the coil-generated magnetic field.

infeasible to scan systematically when dealing with many objectives). The ease of use for this tool must also be emphasized: in each application shown, the deflation algorithm simply was a repeated call to the original optimization or equilibrium problem with a modified objective or augmented with an additional constraint, requiring minimal extra effort to implement and yielding excellent results.

For equilibrium studies, this work showed that deflation methods can be leveraged to find multiple local minima to the near-axis-constrained equilibrium problem, revealing entire families of possible initial guesses which share desirable core characteristics. Deflated equilibrium solves were also used to obtain perturbed helical core equilibria without the need to presciently prescribe the perturbation, showing deflation’s utility in finding bifurcated equilibrium states. These techniques can be applied to any equilibrium problem, so one could imagine modifying another equilibrium code like the Stepped Pressure Equilibrium Code (Hudson *et al.* 2012; Qu *et al.* 2020) to include such methods, where the different equilibrium model and lack of nested surface assumption may permit more interesting bifurcated states to be found.

In stellarator optimization, deflation was used to find multiple distinct and attractive local minima to the stage-one QH optimization problem and the stage-two coil optimization problem, utilizing both conventional deflation operators as well as a novel sum-reduction deflation operator. This showcases deflation’s potential to aid in searching the complex, multi-objective landscapes which characterize stellarator optimization. The deflated optimization in this work is straightforward to implement, and can be easily incorporated into other optimization software (Landreman *et al.* 2021; Zhu *et al.* 2018b; Drevlak *et al.* 2019). Additionally, given that stage-one and stage-two optimization problems are nonconvex, it is only natural that the combined single-stage problem shares this characteristic. The sensitivity of the result to the weights of the objectives in single-stage optimization is even higher (Jorge *et al.* 2023, 2024), and deflation may be useful to find multiple local minima in this case.

There are multiple avenues of improvement to the deflation methods shown in this work. While the specific implementation chosen for this paper is effective and yields pos-

itive results, an improved formulation for least-squares minimization problems following that of Riley *et al.* (2025) would likely yield a more robust deflation method that can successfully converge to higher numbers of distinct solutions, and so will be pursued in future work. These improvements would come from the modified deflated least-squares algorithm being allowed to choose when to take steps which reduce the deflated problem residual and when to take steps which reduce only the undeflated residual when far from known solutions, something which the current implementation's baking the deflation into the objective or constraints does not allow.

Combating the non-uniqueness of the Fourier representation of both coils and surfaces would also improve deflation. While extremely versatile, the Fourier representation suffers from both the issue of parametrization degeneracy, as highlighted earlier in this work, and allowing non-physical, self-intersecting surfaces, both of which render the deflated optimization problem more difficult. The stellarator optimization problem itself would benefit from advances in surface parametrization which improve upon these flaws, and these benefits would apply as well to the effectiveness of deflation in ensuring that mathematically distinct deflated solutions found are also physically distinct. Recent work by Jang *et al.* (2025) on incorporating the expected exponential scaling of such a representation into the optimization process already has been shown to help with these aspects, and indeed was utilized in this paper, but further work is still warranted. For example, the exponential decay of the Fourier representation means that the unweighted  $L^2$  norm used in this deflation work is dominated by the lower-order modes of the state, essentially discouraging solutions which may have similar low order shaping but significantly different higher order shaping. One could instead use an ESS-weighted norm which would more equally weigh the higher-order parts of the state, allowing such solutions to be found.

It could also be interesting to explore deflation not on the state directly, but rather some reduced state or some derived quantities of the state, which may avoid the potential degeneracies associated with the Fourier representation. As an example, one could imagine using an equilibrium's mean rotational transform, minimum magnetic well, and minimum  $L_{\nabla B}$  on the surface as a sort of reduced state for a stellarator. While certainly not a unique identifier for a stellarator, if one is considering tradeoffs in an optimization space, distinct solutions of interest would certainly have differing values for these quantities. One could imagine a best-case scenario where some solutions found using deflation on this reduced state end up being distinct points on the Pareto front between, say, magnetic well and  $L_{\nabla B}$ , for instance. Or, one could take inspiration from NAE theory and use just an equilibrium's axis shape (similar to what was done in Subsection 3.2) and other near-axis quantities, which from the NAE perspective has been shown to discriminate between distinct designs (Rodriguez *et al.* 2023; Landreman 2022).

Finally, further scans over the deflation method hyperparameters and operator types would be useful to probe the sensitivity of the method's effectiveness to the chosen hyperparameters. The hyperparameters  $p$ ,  $\sigma$  (for deflated equilibrium problem), and  $r$  (the additional hyperparameter for deflated constrained optimization) can be tuned to modify the space of found solutions, as well as the deflation operator types: sum versus product, single-shift versus multiple-shift, and norm-deflation versus exponential-deflation (Riley *et al.* 2025). If there is significant sensitivity, as was suggested by preliminary scans during this work, it would actually be a positive outcome, as one may merely use different hyperparameter choices to more broadly search the optimization or solution landscape. Deflation could also be paired with conventional methods of multiple initial conditions or systematic weight scans to increase the effectiveness of each.

## 6. Data Availability

The deflation methods shown in this paper are available at the DESC github repository (Dudt *et al.* 2022). The scripts used are available upon request to the author.

## 7. Acknowledgments

One of the authors (D.P.) acknowledges useful discussions with Elizabeth Paul, Rogerio Jorge, Alan Kaptanoglu, Frank Fu, and Pedro Gil on possible applications of deflation techniques to stellarator optimization. This work is funded through the SciDAC program by the US Department of Energy, Office of Fusion Energy Science and Office of Advanced Scientific Computing Research under contract number DE-AC02-09CH11466, DE-SC0022005, and by the Simons Foundation/SFARI (560651). The United States Government retains a non-exclusive, paid-up, irrevocable, world-wide license to publish or reproduce the published form of this manuscript, or allow others to do so, for United States Government purposes.

## REFERENCES

BINDEL, DAVID, LANDREMAN, MATT & PADIDAR, MISHA 2023 Understanding Trade-offs in Stellarator Design with Multi-objective Optimization. ArXiv:2304.08698 [physics].

BOOZER, ALLEN H 1983 Transport and isomorphic equilibria p. 5, tex.ids=boozer\_transport\_1983-1.

BOOZER, ALLEN H. 2005 Physics of magnetically confined plasmas. *Reviews of Modern Physics* **76** (4), 1071–1141, publisher: American Physical Society.

BROWN, KENNETH M. & GEARHART, WILLIAM B. 1971 Deflation techniques for the calculation of further solutions of a nonlinear system. *Numerische Mathematik* **16** (4), 334–342.

CONLIN, RORY, DUDT, DANIEL W., PANICI, DARIO & KOLEMEN, EGEMEN 2023 The DESC stellarator code suite. Part 2. Perturbation and continuation methods. *Journal of Plasma Physics* **89** (3), 955890305.

CONLIN, RORY, KIM, PATRICK, DUDT, DANIEL W., PANICI, DARIO & KOLEMEN, EGEMEN 2024 Stellarator Optimization with Constraints. ArXiv:2403.11033 [physics].

COOPER, W. A., GRAVES, J. P., POCHELON, A., SAUTER, O. & VILLARD, L. 2010 Tokamak Magnetohydrodynamic Equilibrium States with Axisymmetric Boundary and a 3D Helical Core. *Physical Review Letters* **105** (3), 035003.

DREVLAK, M., BEIDLER, C.D., GEIGER, J., HELANDER, P. & TURKIN, Y. 2019 Optimisation of stellarator equilibria with ROSE. *Nuclear Fusion* **59** (1), 016010, publisher: IOP Publishing.

DUDT, D. W., CONLIN, R., PANICI, D. & KOLEMEN, E. 2023 The DESC stellarator code suite Part 3: Quasi-symmetry optimization. *Journal of Plasma Physics* **89** (2), 955890201, publisher: Cambridge University Press.

DUDT, D. W. & KOLEMEN, E. 2020 DESC: A stellarator equilibrium solver: Physics of Plasmas: Vol 27, No 10 .

DUDT, D. W., CONLIN, D., PANICI, UNALMIS, K., KIM, P. & KOLEMEN, E. 2022 Desc. <https://github.com/PlasmaControl/DESC>.

FARRELL, P. E., BIRKISSON, Á. & FUNKE, S. W. 2015 Deflation Techniques for Finding Distinct Solutions of Nonlinear Partial Differential Equations. *SIAM Journal on Scientific Computing* **37** (4), A2026–A2045, publisher: Society for Industrial and Applied Mathematics.

FREIDBERG, JEFFREY P. 2014 *Ideal MHD*. New York: Cambridge University Press.

GARREN, D. A. & BOOZER, A. H. 1991 Magnetic field strength of toroidal plasma equilibria. *Physics of Fluids B: Plasma Physics* **3** (10), 2805–2821, publisher: American Institute of Physics.

GIL, PEDRO F., KAPTANOGLU, ALAN A. & STENSON, EVE V. 2025 Augmented Lagrangian methods produce cutting-edge magnetic coils for stellarator fusion reactors. ArXiv:2507.12681 [physics].

GREENE, J M 1998 A BRIEF REVIEW OF MAGNETIC WELLS p. 15.

HAM, C.J. & FARRELL, P.E. 2024 On multiple solutions of the Grad–Shafranov equation. *Nuclear Fusion* **64** (3), 034001, publisher: IOP Publishing.

HELANDER, PER 2014 Theory of plasma confinement in non-axisymmetric magnetic fields. *Reports on Progress in Physics* **77** (8), 087001, publisher: IOP Publishing.

HELANDER, P. & SIMAKOV, A. N. 2008 Intrinsic Ambipolarity and Rotation in Stellarators. *Physical Review Letters* **101** (14), 145003, publisher: American Physical Society.

HENNEBERG, SOPHIA A., HELANDER, PER & DREVLAK, MICHAEL 2021 Representing the boundary of stellarator plasmas. *arXiv:2105.00768 [physics]* ArXiv: 2105.00768.

HIRSHMAN, S. P. & BRESLAU, J. 1998 Explicit spectrally optimized Fourier series for nested magnetic surfaces. *Physics of Plasmas* **5** (7), 2664–2675, publisher: American Institute of Physics.

HIRSHMAN, S. P. & WHITSON, J. C. 1983 Steepest-descent moment method for three-dimensional magnetohydrodynamic equilibria. *The Physics of Fluids* **26** (12), 3553–3568, publisher: American Institute of Physics.

HUDSON, S. R., DEWAR, R. L., DENNIS, G., HOLE, M. J., MCGANN, M., VON NESSI, G. & LAZERSON, S. 2012 Computation of multi-region relaxed magnetohydrodynamic equilibria. *Physics of Plasmas* **19** (11), 112502, publisher: American Institute of Physics.

JANG, BYOUNGCHAN, CONLIN, RORY & LANDREMAN, MATT 2025 Exponential Spectral Scaling: Robust and Efficient Stellarator Boundary Optimization via Mode-Dependent Scaling. ArXiv:2509.16320 [physics].

JORGE, R., GIULIANI, A. & LOIZU, J. 2024 Simplified and Flexible Coils for Stellarators using Single-Stage Optimization. ArXiv:2406.07830 [physics].

JORGE, R., GOODMAN, A., LANDREMAN, M., RODRIGUES, J. & WECHSUNG, F. 2023 Single-Stage Stellarator Optimization: Combining Coils with Fixed Boundary Equilibria. *Plasma Physics and Controlled Fusion* **65** (7), 074003, arXiv:2302.10622 [physics].

KAPPEL, JOHN, LANDREMAN, MATT & MALHOTRA, DHAIRYA 2024 The magnetic gradient scale length explains why certain plasmas require close external magnetic coils. *Plasma Physics and Controlled Fusion* **66** (2), 025018, publisher: IOP Publishing.

KAPTANOGLU, ALAN A., WIEDMAN, ALEXANDER, HALPERN, JACOB, HURWITZ, SIENA, PAUL, ELIZABETH J. & LANDREMAN, MATT 2025 Reactor-scale stellarators with force and torque minimized dipole coils. *Nuclear Fusion* **65** (4), 046029, publisher: IOP Publishing.

LAIA, R., JORGE, R. & ABREU, G. 2026 Data-driven approach to model the influence of magnetic geometry in the confinement of fusion devices. *Nuclear Fusion* **66** (1), 016034.

LANDREMAN, MATT 2021 Figures of merit for stellarators near the magnetic axis. *Journal of Plasma Physics* **87** (1), 905870112, tex.ids= landreman\_figures\_2021.

LANDREMAN, MATT 2022 Mapping the space of quasisymmetric stellarators using optimized near-axis expansion. ArXiv:2209.11849 [physics].

LANDREMAN, MATT & BOOZER, ALLEN H. 2016 Efficient magnetic fields for supporting toroidal plasmas. *Physics of Plasmas* **23** (3), 032506, publisher: American Institute of Physics.

LANDREMAN, MATT & JORGE, ROGERIO 2020 Magnetic well and Mercier stability of stellarators near the magnetic axis. *Journal of Plasma Physics* **86** (5), 905860510.

LANDREMAN, MATT, MEDASANI, BHARAT, WECHSUNG, FLORIAN, GIULIANI, ANDREW, JORGE, ROGERIO & ZHU, CAOXIANG 2021 SIMSOPT: A flexible framework for stellarator optimization. *Journal of Open Source Software* **6** (65), 3525.

LANDREMAN, MATT & PAUL, ELIZABETH 2022 Magnetic Fields with Precise Quasisymmetry for Plasma Confinement. *Physical Review Letters* **128** (3), 035001.

MERCIER, CLAUDE 1964 Equilibrium and stability of a toroidal magnetohydrodynamic system in the neighbourhood of a magnetic axis. *Nuclear Fusion* **4** (3), 213–226.

NOCEDAL, JORGE & WRIGHT, STEPHEN J 1999 *Numerical optimization*. Springer.

PANICI, D., CONLIN, R., DUDT, D.W., UNALMIS, K. & KOLEMEN, E. 2023 The DESC stellarator code suite. Part 1. Quick and accurate equilibria computations. *Journal of Plasma Physics* **89** (3), 955890303.

PANICI, DARIO, CONLIN, RORY, GAUR, RAHUL, DUDT, DANIEL W., ELMACIOGLU, YIGIT GUNSUR, LANDREMAN, MATT, ELDER, TODD, SNIR, NADAV, GISSIS, ITAY, NIKULSHIN, YASHA & KOLEMEN, EGEMEN 2025a Surface Current Optimization and Coil-Cutting Algorithms for Stage-Two Stellarator Optimization. ArXiv:2508.09321 [physics].

PANICI, DARIO, RODRIGUEZ, EDUARDO, CONLIN, RORY, DUDT, DANIEL & KOLEMEN, EGEMEN 2025b Extending near-axis equilibria in DESC.

PAPADOPOULOS, IOANNIS P. A., FARRELL, PATRICK E. & SUROWIEC, THOMAS M. 2021 Computing Multiple Solutions of Topology Optimization Problems. *SIAM Journal on Scientific Computing* **43** (3), A1555–A1582, publisher: Society for Industrial and Applied Mathematics.

PENTLAND, K., AMORISCO, N. C., FARRELL, P. E. & HAM, C. J. 2025 Multiple solutions to the static forward free-boundary Grad-Shafranov problem on MAST-U. ArXiv:2503.05674 [physics].

QU, Z S, DEWAR, R L, EBRAHIMI, F, ANDERSON, J K, HUDSON, S R & HOLE, M J 2020 Stepped pressure equilibrium with relaxed flow and applications in reversed-field pinch plasmas. *Plasma Physics and Controlled Fusion* **62** (5), 054002.

RILEY, ALBAN BLOOR, WEBB, MARCUS & BAKER, MICHAEL L. 2025 Deflation Techniques for Finding Multiple Local Minima of a Nonlinear Least Squares Problem. ArXiv:2409.14438 [math].

RODRIGUEZ, EDUARDO, SENGUPTA, WRICK & BHATTACHARJEE, AMITAVA 2023 Constructing the space of quasisymmetric stellarators. ArXiv:2204.10234 [physics].

RODRÍGUEZ, E., PAUL, E. J. & BHATTACHARJEE, A. 2022 Measures of quasisymmetry for stellarators. *Journal of Plasma Physics* **88** (1), 905880109, publisher: Cambridge University Press.

TAREK, MOHAMED & HUANG, YIJIANG 2022 Simplifying deflation for non-convex optimization with applications in Bayesian inference and topology optimization. ArXiv:2201.11926 [math].

WECHSUNG, FLORIAN, LANDREMAN, MATT, GIULIANI, ANDREW, CERFON, ANTOINE & STADLER, GEORG 2022 Precise stellarator quasi-symmetry can be achieved with electromagnetic coils. *Proceedings of the National Academy of Sciences* **119** (13), e2202084119, publisher: Proceedings of the National Academy of Sciences.

WILKINSON, J. H. 1963 *Rounding errors in algebraic processes*. Englewood Cliffs, N.J.: Prentice-Hall, also published by Her Majesty's Stationery Office, London, 1963. Reprinted by Dover, New York, 1994 and SIAM, 2023.

ZHU, CAOXIANG, HUDSON, STUART R., SONG, YUNTAO & WAN, YUANXI 2018a Designing stellarator coils by a modified Newton method using FOCUS. *Plasma Physics and Controlled Fusion* **60** (6), 065008, publisher: IOP Publishing.

ZHU, CAOXIANG, HUDSON, STUART R., SONG, YUNTAO & WAN, YUANXI 2018b New method to design stellarator coils without the winding surface. *Nuclear Fusion* **58** (1), 016008.

## Appendix A. Further Physics Metrics for the Multiple QA NAE-constrained Solutions

In this appendix we share some additional plots of various metrics for the 25 QA first-order NAE-constrained solutions shown in 3.1. Figure 11a shows the magnetic well stability parameter (Greene 1998; Landreman & Jorge 2020; Mercier 1964) across  $\rho$  for each solution, where it can be seen that most solutions have negative wells, indicating instability. However, a few solutions have marginal or even stable magnetic wells for part of the volume, which may be good initial points from which to perform further optimizations. Figure 11b shows the minimum of the  $L_{\nabla B}$  metric (Landreman 2021, 2022) on the boundary of each solution, which Kappel *et al.* (2024) showed is positively correlated with larger feasible coil-plasma distances.

Since these solutions were constrained only to first-order to match the NAE, there was no constraint on these second-order quantities, so the values are essentially uncontrolled during the optimization process. Further work is warranted to perform similar optimizations using higher-order NAE-constrained equilibria, which may restrict the space of possible solutions to a subspace with more favorable properties.

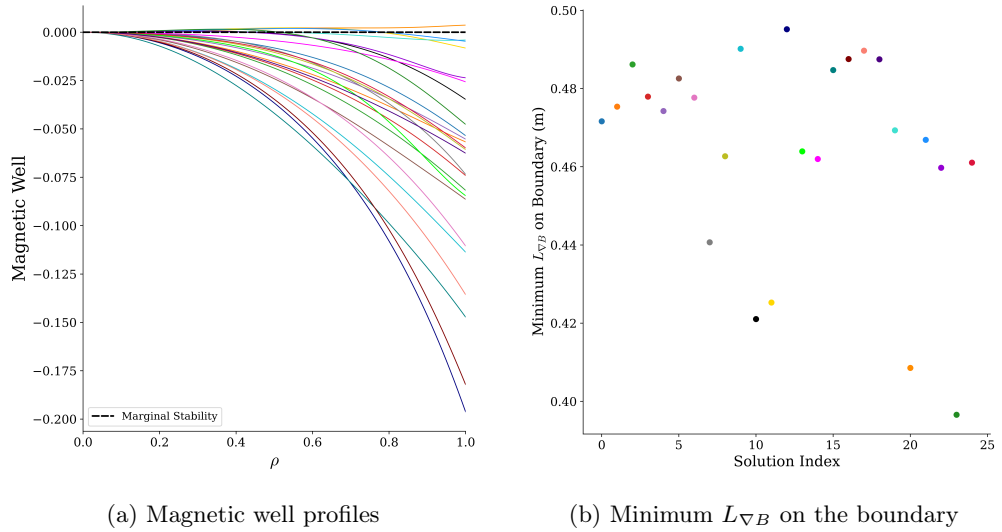


Figure 11: Magnetic well and minimum  $L_{\nabla B}$  on the boundary for the 25 deflated first-order NAE-constrained equilibria.